

# Self-gravitating fluid dynamics, instabilities and solitons

B. Semelin<sup>(a)</sup>, N. Sánchez<sup>(a)</sup>, H. J. de Vega<sup>(b)</sup>

(a) *Observatoire de Paris, Demirm, 61, Avenue de l'Observatoire,  
75014 Paris, FRANCE. Laboratoire Associé au CNRS UA 336,  
Observatoire de Paris et École Normale Supérieure.*

(b) *Laboratoire de Physique Théorique et Hautes Energies,  
Université Paris VI, Tour 16, 1er étage, 4, Place Jussieu 75252 Paris,  
Cedex 05, FRANCE. Laboratoire Associé au CNRS UMR 7589*

(Dated: June 30, 2021)

This work studies the hydrodynamics of self-gravitating compressible isothermal fluids. We show that the hydrodynamic evolution equations are scale covariant in absence of viscosity. Then, we study the evolution of the time-dependent fluctuations around singular and regular isothermal spheres. We linearize the fluid equations around such stationary solutions and develop a method based on the Laplace transform to analyze their dynamical stability. We find that the system is stable below a critical size ( $X \sim 9.0$  in dimensionless variables) and unstable above; this criterion is the same as the one found for the thermodynamic stability in the canonical ensemble and it is associated to a center-to-border density ratio of 32.1. We prove that the value of this critical size is independent of the Reynolds number of the system. Furthermore, we give a detailed description of the series of successive dynamic instabilities that appear at larger and larger sizes following the geometric progression  $X_n \sim 10.7^n$ ,  $n = 1, 2, \dots$ . Then, we search for exact solutions of the hydrodynamic equations without viscosity: we provide analytic and numerical axisymmetric soliton-type solutions. The stability of exact solutions corresponding to a collapsing filament is studied by computing linear fluctuations. Radial fluctuations growing faster than the background are found for all sizes of the system. However, a critical size ( $X \sim 4.5$ ) appears, separating a weakly from a strongly unstable regime.

## I. INTRODUCTION AND RESULTS

Understanding the dynamics of self-gravitating fluids is a fundamental issue in astrophysics. Indeed, the structure of the interstellar medium as well as the formation and evolution of cosmological structures are based on it. Compressible self-gravitating fluid mechanics plays a key role in both star formation and in the formation of a fractal structure for the interstellar medium[1].

Self-gravitating systems can be studied at different levels. The first is purely thermodynamic. It leads to the description of their states of equilibrium and the study of their stability. This approach has been followed in the case of the isothermal sphere configuration [2, 3, 4, 5, 6] leading to the description of the gravothermal instability. This behaviour appears when the size of the sphere goes above a critical size, or, for a given size, when its temperature drops below a critical temperature. An instability develops and the system collapses to a dense core. In refs.[9, 10, 11, 12] the statistical mechanics of the self-gravitating gas has been investigated with analytic (saddle point in the functional integral) as well as Monte Carlo methods. In addition to the thermodynamics, this approach provides the exact equation of state of the self-gravitating gas[12].

The dynamics can be studied from the hydrodynamic equations of a self-gravitating fluid. This is a set of non-linear partial differential equations and exact solutions can be found only under simplifying hypotheses. For example, the case of one space dimension has been studied in ref.[13] and the axisymmetric case in ref.[14].

Finally, the last approach to the study of self-gravitating systems is numerical, it has been widely followed[8].

In this paper we study the hydrodynamics of a self-gravitating fluid. We show that the hydrodynamic evolution equations for a self-gravitating fluid are **covariant under scale transformations** in absence of viscosity. That is, if we scale the space and time variables by a constant factor in a solution of the fluid equations, we get again a solution of the equations.

We consider the Navier-Stokes equation for an isothermal self-gravitating fluid and restrict our study to potential flows. Within these hypotheses we show that a Reynolds number appears as the only parameter that breaks the scale covariance in the Navier-Stokes equation. Moreover we find that a characteristic density enters the Reynolds number definition, implying that a system with no characteristic density has no characteristic Reynolds number; the flow is then scale covariant.

In section III we present a general method for the analysis of linear dynamic stability of stationary solutions of the equations. This method is based on the Laplace transform in time of the evolution equations. The functional determinant of the Laplace transformed operator is studied as a function of  $s$  (the Laplace transform parameter). Its zeros in the  $s$ -plane determine whether the solution is stable or not. Unstable solutions yield zeroes with positive

real part while purely imaginary zeros or zeroes with negative real part correspond to stable solutions (oscillating or damped). We apply this analysis to isothermal spheres where we first specify the initial data and the boundary conditions.

In section IV, using the Laplace transform, we derive the analytic form of the fluctuations in the case of a singular isothermal sphere background. Then, we show that the boundary conditions build a discret spectrum of proper modes for the system. The stability of these modes is decided by the complex value of their pulsations in the Laplace transform plane. We then apply a general numerical method based on finite differences to both the singular and the regular isothermal sphere cases and compute the pulsations as functions of the size of the system. We show that in both cases the dynamic stability depends on the size of the system. Under a critical size  $X_{c_1}$  the system is stable, while above it becomes unstable. In dimensionless variables this size is  $X_{c_1} \sim 10.7 \delta$  in the singular case ( $\delta$  is the short distance cutoff necessary in this case) and  $X_{c_1} \sim 9.0$  in the regular case. This critical size is the same as the one found in thermodynamic studies in the canonical ensemble (we used boundary conditions connected to the canonical ensemble). It is often expressed as a critical center-to-border density contrast whose value is 32.1 for the regular isothermal sphere. However, we also show how secondary instabilities  $X_{c_2}, \dots, X_{c_n}$  appear at larger sizes. These sizes follow the geometric progression  $10.7^n$  ( $n = 1, 2, \dots$ ) in the singular case and do so asymptotically ( $n \gg 1$ ) in the regular case. The density and velocity profiles of the two first instabilities are given. Figs. 1-3 show these profiles and the spectrum of modes for the regular and singular spheres.

In section V we include the viscosity in the fluid equations. Then, we study the influence of the Reynolds number on the stability criterion. The result is that the critical sizes at which the instable modes appear are **independent** of the Reynolds number. The complicated evolution of the pulsations of the modes as functions of both the system size and the Reynolds number is plotted in figs. 4-6.

In section VI we turn to time-dependent background solutions. We look for axisymmetric soliton-type solutions. We define a soliton variable:

$$y = \frac{\mu r}{1 \pm \mu c_s t}, \quad (1.1)$$

where  $\mu$  is an inverse characteristic length ( $\mu^{-1}$  is the Jeans' length),  $c_s$  the sound speed,  $r$  the polar radius and  $t$  the time. We reduce the equations to a single non-linear equation and we find non-trivial solutions such as,

$$v_r = \pm c_s \left( \sqrt{C} + \frac{\mu r}{1 \pm \mu c_s t} \right), \quad \Phi = \ln \left[ \frac{\sqrt{C}}{\mu^2 r^2 (1 \pm \mu c_s t)} \right]. \quad (1.2)$$

This solution describes an expanding or collapsing filament depending on the choice for  $\pm$ . Other background solutions are described. Then, explicit radial fluctuations around the solution (1.2) are computed and their stability is analyzed with the same method as for the isothermal spheres. Some of the modes appear to grow faster than the background whatever the size of the system. A specific size,  $X_{c_1} \sim 4.5 \delta$ , marks the appearance of faster growing fluctuations at larger sizes. However, these are radial fluctuations invariant along the axis of the symmetry; consequently they have an infinite mass for all radial sizes of the system. Limitating the size of the system along the symmetry axis should provide a stable behaviour for small enough sizes.

Section VII is devoted to our conclusions and final remarks.

## II. THE NAVIER-STOKES EQUATION FOR SELF-GRAVITATING FLUIDS

The evolution of a self-gravitating, isothermal fluid is described by a density field,  $\rho(\mathbf{r}, t)$ , a pressure field  $P(\mathbf{r}, t)$ , a gravitational potential  $U(\mathbf{r}, t)$  and a velocity field  $\mathbf{v}(\mathbf{r}, t)$ . These four fields obey four equations: the matter conservation, the Navier-Stokes equation, the Poisson equation and the equation of state[7], respectively given by

$$\frac{\partial \rho}{\partial t} + \nabla \cdot (\rho \mathbf{v}) = 0, \quad (2.1)$$

$$\frac{\partial \mathbf{v}}{\partial t} + (\mathbf{v} \cdot \nabla) \mathbf{v} = -\frac{\nabla P}{\rho} - \nabla U + \frac{\eta}{\rho} \nabla^2 \mathbf{v} + \frac{1}{\rho} \left( \zeta + \frac{\eta}{3} \right) \nabla (\nabla \cdot \mathbf{v}), \quad (2.2)$$

$$\nabla^2 U = 4\pi G \rho, \quad (2.3)$$

$$c_s^2 = \frac{\partial P}{\partial \rho}. \quad (2.4)$$

Here  $\zeta$  and  $\eta$  stand for the kinematical viscosity coefficients and  $c_s$  is the speed of sound. We assume  $c_s$  to be a constant which corresponds to the equation of state of a perfect gas.

From now on, we restrict for simplicity to potential flows, which implies the existence of a velocity potential  $\Psi$ . In order to work with dimensionless variables we define  $\mu$ , the inverse of a characteristic length, as:

$$\mu^2 = \frac{4\pi G \rho_0}{c_s^2}. \quad (2.5)$$

where  $\rho_0$  is a characteristic density of the system.

We then introduce dimensionless variables and fields :

$$\begin{aligned} \mathbf{x} &= \mu \mathbf{r} \quad , \quad \tau = \mu c_s t \quad , \\ \Phi &= \ln \frac{\rho}{\rho_0} \quad , \quad \mathbf{v} = \frac{c_s}{\mu} \nabla_{\mathbf{x}} \Psi(\mathbf{x}, \tau) \quad . \end{aligned} \quad (2.6)$$

Here,  $\nabla_{\mathbf{x}}$  is the derivative with respect to the dimensionless coordinate  $\mathbf{x}$ . We can take advantage of the potential nature of the velocity field to simplify the dissipation term in the Navier-Stokes equation. Moreover, to be able to eliminate the field  $U$ , we now take the divergence of Navier-Stokes equation. At the same time, to get an equivalent formulation, we must take the rotational of Navier-Stokes equation. This last constraint yields the simple equation (2.9) for non-zero viscosity. It disappears for flows with zero viscosity. The system can now be described with the variables  $\Phi$  and  $\Psi$  only as follows

$$\partial_\tau \nabla^2 \Psi + (\nabla \Psi \nabla) \nabla \Psi = -\nabla^2 \Phi - e^\Phi + \frac{1}{Re} \nabla \cdot [e^{-\Phi} \nabla (\nabla^2 \Psi)] \quad , \quad (2.7)$$

$$\partial_\tau \Phi + \nabla^2 \Psi + \nabla \Phi \cdot \nabla \Psi = 0, \quad (2.8)$$

$$\nabla \Phi \wedge \nabla (\nabla^2 \Psi) = 0, \quad (2.9)$$

$$\frac{1}{Re} = \left( \frac{4}{3} \eta + \zeta \right) \frac{\mu}{\rho_0 c_s} \quad . \quad (2.10)$$

$Re$  is the analogous of the usual Reynolds number for the compressible self-gravitating flow.

Now, let us see that the flow is scale covariant in the absence of viscosity. This can be proven as follows. Assume that  $\{\Phi(\mathbf{x}, \tau), \Psi(\mathbf{x}, \tau)\}$  is a solution of eqs.(2.7)-(2.9). We then define the scale-transformed fields as

$$\begin{aligned} \Phi_\lambda(\mathbf{x}, \tau) &= \Phi(\lambda \mathbf{x}, \lambda \tau) + \ln \lambda^2 \quad , \\ \Psi_\lambda(\mathbf{x}, \tau) &= \lambda^{-1} \Psi(\lambda \mathbf{x}, \lambda \tau) \quad . \end{aligned} \quad (2.11)$$

Using that

$$\begin{aligned} \frac{\partial \Phi_\lambda}{\partial x_k} &= \lambda \frac{\partial \Phi}{\partial y_k} \quad , \quad \frac{\partial \Phi_\lambda}{\partial \tau} = \lambda \frac{\partial \Phi}{\partial \tilde{\tau}} \quad , \\ \frac{\partial \Psi_\lambda}{\partial x_k} &= \frac{\partial \Psi}{\partial y_k} \quad , \quad \frac{\partial \Psi_\lambda}{\partial \tau} = \frac{\partial \Psi}{\partial \tilde{\tau}} \quad , \end{aligned} \quad (2.12)$$

where  $y_k \equiv \lambda x_k$  and  $\tilde{\tau} \equiv \lambda \tau$ , we obtain that  $\Phi_\lambda(\mathbf{x}, \tau)$ ,  $\Psi_\lambda(\mathbf{x}, \tau)$  is also a solution of eqs.(2.7)-(2.8) for  $Re = \infty$ . The transformation (2.11) generalizes to the time dependent case the scale transformation for  $\Phi(\mathbf{x})$  found in ref.[10] in the hydrostatic case.

We find from eqs.(2.6) and (2.11) that the velocity field transforms as,

$$\mathbf{v}_\lambda(\mathbf{x}, \tau) = \mathbf{v}(\lambda \mathbf{x}, \lambda \tau) \quad .$$

Under this transformation, all terms in eq.(2.8) scale as  $\lambda$  and in eq.(2.7) as  $\lambda^2$  except for the last (viscous) term in eq.(2.7) that scales as  $\lambda$ . Therefore, for  $\lambda \rightarrow \infty$  scale invariance is recovered. This corresponds to the long wavelength limit as one could expect.

When the flow is a fluctuation, for example, a fluctuation around an isothermal sphere with a characteristic central density, the scale invariance is broken. However, in this case we will see that it is recovered asymptotically at large distances.

### III. THE DYNAMIC STABILITY OF ISOTHERMAL SPHERES

We study in this section the evolution of time dependent fluctuations around an isothermal sphere. We linearize the fluid equations (2.7)-(2.9) around such exact static solutions and apply Laplace transform to solve them.

#### A. Linearization

Equation (2.7) and (2.8) have well-known static spherically symmetric solutions: the isothermal spheres. These are the solutions of the equations:

$$\frac{d^2\Phi_0}{dx^2} + \frac{2}{x} \frac{d\Phi_0}{dx} + e^{\Phi_0} = 0 , \quad (3.1)$$

$$\Psi_0 = 0 , \quad (3.2)$$

where  $x$  is the dimensionless radius  $\mu r$ . These solutions are studied in [2, 5, 6, 12]. Stable isothermal spheres have a finite radius. Solutions of eq.(3.1) reaching infinite radial distance suppose an infinite total mass. Therefore, we shall consider the fluid confined in a spherical box of finite size.

The thermodynamic stability of isothermal spheres has been extensively studied, leading to the discovery of the gravo-thermal instability ([3], [4] and [5]). Our aim is to investigate the dynamic instability of these states and compare with the thermodynamic results [12]. To achieve the stability analysis we introduce fluctuations around the isothermal spheres:

$$\Phi(\mathbf{x}, \tau) = \Phi_0 + \epsilon \phi(\mathbf{x}, \tau) , \quad (3.3)$$

$$\Psi(\mathbf{x}, \tau) = \epsilon \psi(\mathbf{x}, \tau) , \quad (3.4)$$

where  $\epsilon$  is a small parameter.

We can then write the linearized system where only first order contributions in  $\epsilon$  are kept:

$$\partial_\tau \nabla^2 \psi(\mathbf{x}, \tau) = -\nabla^2 \phi(\mathbf{x}, \tau) - e^{\Phi_0(x)} \phi(\mathbf{x}, \tau) + \frac{1}{Re} \nabla \cdot [e^{-\Phi_0(x)} \nabla (\nabla^2 \psi(\mathbf{x}, \tau))] , \quad (3.5)$$

$$\partial_\tau \phi(\mathbf{x}, \tau) + \nabla^2 \psi(\mathbf{x}, \tau) + \nabla \Phi_0(x) \cdot \nabla \psi(\mathbf{x}, \tau) = 0 , \quad (3.6)$$

$$\nabla \Phi_0 \wedge \nabla (\nabla^2 \psi) = 0 . \quad (3.7)$$

Since we study fluctuations around a spherically symmetric solution, it is natural to expand  $\psi(\mathbf{x}, \tau)$  and  $\phi(\mathbf{x}, \tau)$  in spherical harmonics. Let us write first,

$$\phi(\mathbf{x}, \tau) = \sum_{l,m} \phi_{l,m}(x, \tau) Y_{l,m}(\theta, \varphi) , \quad (3.8)$$

$$\psi(\mathbf{x}, \tau) = \sum_{l,m} \psi_{l,m}(x, \tau) Y_{l,m}(\theta, \varphi) . \quad (3.9)$$

The action of the laplacian is on  $\phi_{l,m}$  and  $\psi_{l,m}$  is:

$$\nabla^2 = \frac{d^2}{dx^2} + \frac{2}{x} \frac{d}{dx} - \frac{l(l+1)}{x^2} . \quad (3.10)$$

Then, the system of equations can be written as :

$$\nabla^2 \partial_\tau \psi_l(x, \tau) + [\nabla^2 + e^{\Phi_0}] \phi_l(x, \tau) - \frac{1}{Re} \nabla \cdot [e^{-\Phi_0(x)} \nabla (\nabla^2 \psi_l(x, \tau))] = 0, \quad (3.11)$$

$$\partial_\tau \phi_l(x, \tau) + [\nabla^2 + (\partial_x \Phi_0) \partial_x] \psi_l(x, \tau) = 0,$$

$$\sum_{l,m} \nabla^2 \psi_l \partial_\theta Y_{l,m} = 0, \quad \sum_{l,m} \nabla^2 \psi_l \partial_\varphi Y_{l,m} = 0. \quad (3.12)$$

We can see from the last condition that all  $m \neq 0$  modes must be zero. This justifies labeling the radial components of  $\phi$  and  $\psi$  with  $l$  only. Such a cancellation of  $m \neq 0$  modes happens only in the linear approximation. Moreover, the two last conditions are trivial for  $l = 0$ ; the S-wave mode is indeed decoupled from the others. This is not the case however for  $l > 0$  modes, which are coupled through the condition (3.12), if the viscosity is not zero. Consequently, **in the viscous case**, we will restrict ourselves to the study of S-wave perturbations. Since the two last conditions are automatically satisfied within the extend of our study, we will not mention them again.

Analytic solutions will be given in specific cases. We analyze below the system of equations (3.11) by using Laplace transformation in time, showing that this is a powerful approach for a stability analysis.

### B. Laplace transform analysis

We are interested on fields which grow slower than some exponential of time and therefore admit a Laplace transform for some finite  $s > 0$ . This space of solutions is rich enough for our analysis. The Laplace transforms of our fields are defined by:

$$\begin{aligned} \hat{\phi}_l(x, s) &= \int_0^{+\infty} d\tau e^{-s\tau} \phi_l(x, \tau), \\ \hat{\psi}_l(x, s) &= \int_0^{+\infty} d\tau e^{-s\tau} \psi_l(x, \tau). \end{aligned} \quad (3.13)$$

The Laplace transform of the evolution equations (3.11) takes then the form

$$\mathcal{M}(x, s) \begin{pmatrix} \hat{\psi}_l(x, s) \\ \hat{\phi}_l(x, s) \end{pmatrix} = \begin{pmatrix} \nabla^2 \psi_l(x, \tau = 0) \\ \phi_l(x, \tau = 0) \end{pmatrix} \quad (3.14)$$

where

$$\mathcal{M}(x, s) = \begin{bmatrix} s \nabla^2 - \frac{1}{Re} \nabla \cdot (e^{-\Phi_0(x)} \nabla \nabla^2) & \nabla^2 + e^{\Phi_0(x)} \\ \nabla^2 + \partial_x \Phi_0 \partial_x & s \end{bmatrix} \quad (3.15)$$

Indeed, the inverse Laplace transforms can be written :

$$\begin{aligned} \phi_l(x, \tau) &= \int_\Gamma ds \frac{e^{s\tau}}{2\pi i} \hat{\phi}_l(x, s), \\ \psi_l(x, \tau) &= \int_\Gamma ds \frac{e^{s\tau}}{2\pi i} \hat{\psi}_l(x, s). \end{aligned} \quad (3.16)$$

where the contour  $\Gamma$  runs upwards parallel and to the right of the imaginary  $s$  axis. The functions  $\hat{\phi}_l(x, s)$  and  $\hat{\psi}_l(x, s)$  in the integrand of eq.(3.16) are given by the inverse operator  $\mathcal{M}(\cdot, s)^{-1}$  acting on the r.h.s. of eq.(3.14). Hence, the poles of the integrand are given by the zeros  $s_k$ ,  $k = 1, 2, 3, \dots$  of the determinant of the operator  $\mathcal{M}(\cdot, s)$ .

Closing the contour  $\Gamma$  with a path on the  $\text{Res} < 0$  half-plane and computing the integral in eqs.(3.16) by residua we get for the fields a sum of terms associated to the poles of the integrand. Then, we can push the contour in the  $\text{Res} < 0$  half-plane towards  $\text{Res} \rightarrow -\infty$  where its contribution vanishes.

Therefore, the inverse Laplace transforms (3.16) become sum of terms depending on time through  $e^{s_k \tau}$ . If  $s_k$  has a positive real part the mode is unstable, growing exponentially with time.

$$\phi_l(x, \tau) = \sum_{poles} e^{s_k \tau} \text{res} \hat{\phi}_l(x, s_k),$$

$$\psi_l(x, \tau) = \sum_{poles} e^{s_k \tau} \text{res} \hat{\psi}_l(x, s_k) . \quad (3.17)$$

The method for analyzing the stability of the system is now clear: we determine the zeroes of the determinant of our operator  $\mathcal{M}(\cdot, s)$  as a function of  $s$  for various values of  $l$  under specified boundary conditions, and we look for zeroes in the  $\text{Re}(s) > 0$  half-plane of the complex  $s$ -plane.

### C. Boundary conditions on an spherical domain

Regularity at the origin requires,

$$\partial_x \phi_l(x, \tau)|_{x=0} = 0 \quad , \quad \partial_x \psi_l(x, \tau)|_{x=0} = 0 \quad . \quad (3.18)$$

As already mentioned, we confine our system in a spherical box to provide a large distance cut-off. We consider a spherical box of radius  $X$  and we require  $\psi_l$  and the radial velocity to vanish on the surface of the sphere. The first condition has is like a gauge condition and has no physical effect, while the second prevents the fluid from exiting the confining box.

$$\partial_x \psi_l(x, \tau)|_{x=X} = 0 \quad , \quad \psi_l(X, \tau) = 0 \quad . \quad (3.19)$$

These conditions translate for the Laplace transforms into:

$$\partial_x \hat{\phi}_l(0, s) = \partial_x \hat{\psi}_l(0, s) = 0 \quad , \quad \partial_x \hat{\psi}_l(X, s) = \hat{\psi}_l(X, s) = 0$$

Perturbations with non-zero total mass are in fact zero-mass perturbations around an isothermal sphere with a different parameter  $\mu = \mu_1$ . They **must** not be included in the stability study.

We can actually prove that the mass of the field is unchanged to first order by the perturbations. Namely, that the integral

$$\int_0^X \phi(\vec{x}, \tau) e^{\Phi_0(x)} x^2 dx \quad (3.20)$$

identically vanish.

For perturbations with  $l \neq 0$  the integral (3.20) trivially vanishes upon integration over the angles. For  $l = 0$ , we can rewrite the Laplace transform of eq.(3.6) as follows

$$s \hat{\phi}_0(x, s) + e^{-\Phi_0(x)} \nabla \left[ e^{\Phi_0(x)} \nabla \hat{\psi}_0(x, s) \right] = 0$$

Hence, integrating over the sphere,

$$s \int_0^X \hat{\phi}_0(x, s) e^{\Phi_0(x)} x^2 dx = -e^{\Phi_0(x)} \left. \frac{d\hat{\psi}_0(x, s)}{dx} \right|_{x=0}^{x=X} = 0$$

where we used eqs.(3.18)-(3.19).

In order to study the solutions of eqs.(3.14) with the boundary conditions eq.(3.18)-(3.19), let us first reformulate eq.(3.14). We will restrict this study to  $l = 0$ .

Introducing  $f(x, s) = \frac{d\hat{\psi}_0}{dx}$  we can reduce eq. (3.14) to:

$$\begin{aligned} & \frac{d}{dx} \left\{ \left[ 1 + \frac{s}{Re} e^{-\Phi_0(x)} \right] \frac{d^2 f}{dx^2} + \left[ \frac{2}{x} \left( 1 + \frac{s}{Re} e^{-\Phi_0(x)} \right) + \frac{d\Phi_0}{dx} \right] \frac{df}{dx} \right. \\ & - \left. \left[ s^2 + \frac{2}{x^2} \left( 1 + \frac{s}{Re} e^{-\Phi_0(x)} \right) + \frac{2}{x} \frac{d\Phi_0}{dx} \right] f(x, s) \right\} = -s \frac{d^2 \psi_0}{dx^2}(x, \tau = 0) \\ & \hat{\phi}_0(x) = -\frac{1}{s} \left[ \frac{df}{dx}(x, s) + \frac{d\Phi_0}{dx} f(x, s) \right] . \end{aligned} \quad (3.21)$$

We can integrate the total derivative and drop the integration constant thanks to eqs.(3.18)-(3.19). We find,

$$\begin{aligned} & \left[1 + \frac{s}{Re} e^{-\Phi_0(x)}\right] \frac{d^2 f}{dx^2} + \left[\frac{2}{x} \left(1 + \frac{s}{Re} e^{-\Phi_0(x)}\right) + \frac{d\Phi_0}{dx}\right] \frac{df}{dx} \\ & - \left[s^2 + \frac{2}{x^2} \left(1 + \frac{s}{Re} e^{-\Phi_0(x)}\right) + \frac{2}{x} \frac{d\Phi_0}{dx}\right] f(x, s) + s \frac{d\psi_0}{dx}(x, \tau = 0) = 0 \quad . \end{aligned} \quad (3.22)$$

The boundary conditions for  $f(x, s)$  follow from eqs.(3.18)-(3.19):

$$f(0, s) = f(X, s) = 0 \quad . \quad (3.23)$$

Let us first analyze this linear problem in the zero viscosity case, namely  $Re = \infty$ . Eq.(3.22) thus becomes,

$$\frac{d^2 f}{dx^2} + \left[\frac{2}{x} + \frac{d\Phi_0}{dx}\right] \frac{df}{dx} - \left[s^2 + \frac{2}{x^2} + \frac{2}{x} \frac{d\Phi_0}{dx}\right] f(x, s) + s \frac{d\psi_0}{dx}(x, \tau = 0) = 0 \quad (3.24)$$

This ordinary second order differential equation takes a Schrödinger-type form upon the transformation

$$f(x, s) = \frac{e^{-\frac{1}{2} \Phi_0(x)}}{x} w(x, s) \quad .$$

We find for the homogeneous part

$$-\frac{d^2 w}{dx^2}(x, s) + \left[\frac{2}{x^2} + \frac{1}{4} \left(\frac{d\Phi_0}{dx}\right)^2 + \frac{2}{x} \frac{d\Phi_0}{dx} - \frac{1}{2} e^{\Phi_0}\right] w(x, s) = -s^2 w(x, s) \quad (3.25)$$

Here,

$$V(x) \equiv \frac{2}{x^2} + \frac{1}{4} \left(\frac{d\Phi_0}{dx}\right)^2 + \frac{2}{x} \frac{d\Phi_0}{dx} - \frac{1}{2} e^{\Phi_0} = \frac{1}{2} \left(\frac{d\Phi_0}{dx} + \frac{2}{x}\right)^2 - \frac{1}{4} \left(\frac{d\Phi_0}{dx}\right)^2 - \frac{1}{2} e^{\Phi_0}$$

plays the role of the ‘potential’ and  $-s^2$  the role of the ‘energy’ eigenvalue in the Schrödinger-type equation.

Notice that the potential is singular and repulsive at short distances since

$$V(x) \xrightarrow{x \rightarrow 0} \frac{2}{x^2} + \mathcal{O}(1) \quad ,$$

while it is attractive for distances where  $\frac{d\Phi_0}{dx} \sim -2/x$ . In the case of a potential attractive at short distances, or in the case of an infinite domain, a continuous part could appear in the spectrum. In our case (finite domain and repulsive potential), the spectrum will be discrete (see ref.[17] p 445 for a mathematical study). Notice however that the numerical methods used in the sequel can handle both continuous and discrete spectrum.

Thus, imposing the boundary condition  $w(0, s) = w(X, s) = 0$  yields a discrete spectrum of eigenfunctions  $w_n(x)$  with negative eigenvalues  $s_n^2$  plus possibly some eigenvalues with positive  $s_n^2$  corresponding to the ‘bound states’ in eq.(3.25). This ensemble of eigenfunctions form a complete set.

We can now solve the inhomogeneous equation (3.24) by expanding in the eigenfunctions

$$f_n(x) = \frac{e^{-\frac{1}{2} \Phi_0(x)}}{x} w_n(x) \quad ,$$

of the homogeneous problem (3.25) with boundary conditions (3.23) and normalized as

$$\int_0^X x^2 e^{\Phi_0(x)} f_n(x) f_k(x) dx = \delta_{nk} \quad .$$

We thus write

$$f(x, s) = \sum_n c_n(s) f_n(x) \quad (3.26)$$

where the  $c_n(s)$  are for the moment arbitrary. Inserting eq.(3.26) into eq.(3.24), multiplying by  $f_k(x)$  and integrating over  $x$  yields,

$$f(x, s) = s \sum_n \int_0^X \frac{x'^2 e^{\Phi_0(x')}}{s^2 - s_n^2} f_n(x) f_n(x') \frac{d\psi_0}{dx'}(x', \tau = 0) \quad .$$

Thus,  $f(x, s)$  exhibits poles in  $s^2$  at each eigenvalue  $s_n^2$ . Positive  $s_n^2$  describe instabilities as discussed at the end of sec. III C since such poles imply exponentially growing fluctuations as  $e^{|s_n|\tau}$ . Negative eigenvalues  $s_n^2 = -k_n^2$  yield oscillating behaviour  $e^{ik_n\tau}$ .

In the viscous case eq.(3.22) can be reduced to a ‘Schrödinger type’ equation with an energy dependent potential upon the transformation

$$f(x, s) = \frac{e^{-\frac{1}{2}\Phi_0(x)}}{x \sqrt{\alpha_s(x)}} w(x, s) \quad .$$

where

$$\alpha_s(x) = 1 + \frac{s}{Re} e^{-\Phi_0(x)} \quad (3.27)$$

We then find for the homogeneous part,

$$-\frac{d^2 w}{dx^2}(x, s) + \left[ \frac{2}{x^2} + \frac{\left(\frac{d\Phi_0}{dx}\right)^2}{4\alpha_s^2(x)} + \frac{2}{x} \frac{d\Phi_0}{dx} - \frac{e^{\Phi_0(x)}}{2\alpha_s(x)} + \frac{s}{Re} \frac{\left(\frac{d\Phi_0}{dx}\right)^2 e^{-\Phi_0(x)}}{2\alpha_s^2(x)} \right] w(x, s) = -\frac{s^2}{\alpha_s^2(x)} w(x, s)$$

A more mathematical study of the fluctuation equations can be done here in the spirit of ref.[16].

#### IV. THE NON-VISCOUS ISOTHERMAL SPHERES

##### A. Analytical study

The singular isothermal sphere is an analytic solution to eq (3.1) given by,

$$\Phi_0 = \ln \frac{2}{x^2} \quad . \quad (4.1)$$

This solution has an infinite total mass and produces infinite pressure at the center. To avoid this divergence we introduce a short distance cutoff  $\delta$ . The spherical box provides the long distance cutoff. We study the singular sphere background as an analytic model for the regular sphere. In this spirit we rewrite the boundary conditions as:

$$\begin{aligned} \partial_x \hat{\psi}_l(x, s) \Big|_{x=\delta} &= 0 \quad , \quad \partial_x \hat{\phi}_l(x, s) \Big|_{x=\delta} = 0 \quad , \\ \partial_x \hat{\psi}_l(x, s) \Big|_{x=X} &= 0 \quad , \quad \hat{\psi}_l(X, s) = 0 \quad . \end{aligned} \quad (4.2)$$

Conditions at  $x = \delta$  are straightforward translations of conditions at  $x = 0$ .

The advantage of this analytic background solution is that we can write down analytic expressions for the fluctuations. Indeed for  $l = 0$  eq.(3.25) reduces to:

$$\left[ \frac{d^2}{dx^2} + \frac{2}{x^2} - s^2 \right] f(x, s) = 0 \quad , \quad (4.3)$$

where  $f(x, s) = w(x, s)$  in this case, is the dimensionless radial velocity of the  $l = 0$  mode. In dimensionful variables, the radial velocity fluctuations for  $l = 0$  are:

$$\begin{aligned} v_r(r, t) &= c_s \left( A_1 e^{i\omega t} + A_2 e^{-i\omega t} \right) \sqrt{kr} \left[ B_1 J_\nu(kr) + B_2 J_{-\nu}(kr) \right] \quad , \\ s &= ik \quad , \quad \omega^2 = k^2 c_s^2 \quad , \quad \nu = \frac{i\sqrt{7}}{2} \quad . \end{aligned} \quad (4.4)$$

where  $J_\nu(z)$  are Bessel functions. The corresponding fluctuation  $\phi(r, t)$  takes the form



$$\phi(r, t) = (A'_1 e^{i\omega t} + A'_2 e^{-i\omega t}) \sqrt{kr} \left[ B'_1 \frac{dJ_\nu}{dr}(kr) + B'_2 \frac{dJ_{-\nu}}{dr}(kr) \right] . \quad (4.5)$$

The boundary conditions (3.23) yield a system of two homogeneous equations for the constants  $B_1, B_2$ ,

$$\begin{aligned} B_1 J_\nu(kX) + B_2 J_{-\nu}(kX) &= 0 \\ B_1 J_\nu(k\delta) + B_2 J_{-\nu}(k\delta) &= 0 \end{aligned} \quad (4.6)$$

Therefore, in order to have a non-trivial solution we impose the trascendental equation,

$$\frac{J_\nu(kX)}{J_{-\nu}(kX)} = \frac{J_\nu(k\delta)}{J_{-\nu}(k\delta)} \quad (4.7)$$

This equation is fulfilled for specific values of  $k$ , yielding a discret spectrum for the modes.

Real solutions  $k_n$  of eq.(4.7) can be obtained asymptotically using the Mac Mahon expansion [15]. Depending on the value of  $X/\delta$  there can be solutions with real or with imaginary  $k_n$ . The threshold of instabilities precisely appears when the eigenvalues go through  $k = 0$  turning from real to imaginary. In such limit eq.(4.7) yields

$$\sin \left[ \frac{\sqrt{7}}{2} \log \frac{X_c}{\delta} \right] = 0$$

with the exact solutions

$$\frac{X_{cl}}{\delta} = e^{\frac{2\pi l}{\sqrt{7}}} = (10.749\dots)^l, \quad l = 1, 2, 3, \dots$$

Each time  $\frac{X}{\delta}$  crosses each of these thresholds upwards, a new instable eigenvalue appears. The first instability occurs for  $l = 1$ . These points exactly coincide with those found in ref.[11].

We have checked that the general method that we will describe in section (IV B) gives numerically the same results as eqs.(4.4)-(4.7).

## B. Numerical method

The general numerical method, consists in replacing the derivatives by finite differences turning eq.(3.14) and the boundary conditions into a  $N \times N$  ( $N \gg 1$ ) linear system. More specifically,  $\hat{\phi}$  and  $\hat{\psi}$  as functions of  $x$  are represented by their values on a discret set of points  $\{x_k, 1 \leq k \leq N\}$ . The differential operator are then represented by finite differences. Evaluating the differential equation in each point produces an algebraic equation. Boundary conditions provide the missing equations at the boundary of the domain, where the differential operator cannot be evaluated. As explained in section III B, we then evaluate the determinant of the system in a given domain of  $X/\delta$ ,  $s$  and  $Re$  and look for cancellations.

As the parameter domain is huge (four-dimensional), we must limit the number  $N$  in the determinant. It has been set to 40 in most computations. However, different values (up to 200) have been used to investigated the stability of the results around randomly chosen cancellations of the determinant, and more specifically in the region of the stability-instability transition. No ill-behaviour has been detected.

## C. Stability of the singular sphere

Cancellations of the determinant of the differential operator happen for discret values of the parameter  $s$ . If one of these eigenvalues  $s$  has a positive real part, then the associated mode grows with time and the system is unstable. It is known from thermodynamic studies that for a given central density, the stability depends on the size of the sphere. Thus, we will investigate for the zeroes of the determinant in a three-dimensional domain  $(s, X) \in C \times R$ . The zeroes are shown on fig.1 for  $l = 0$ .

The first result of fig.1 is that it shows a symmetry around the  $Re(s) = 0$  axis; we have a set of coupled modes with opposite pulsations. Then, we have checked that the pulsations of the spectrum of modes have purely imaginary values for  $X/\delta$  smaller than a critical value  $X_{c1}/\delta$ . This range of  $X/\delta$  values in mostly outside the domain pictured on

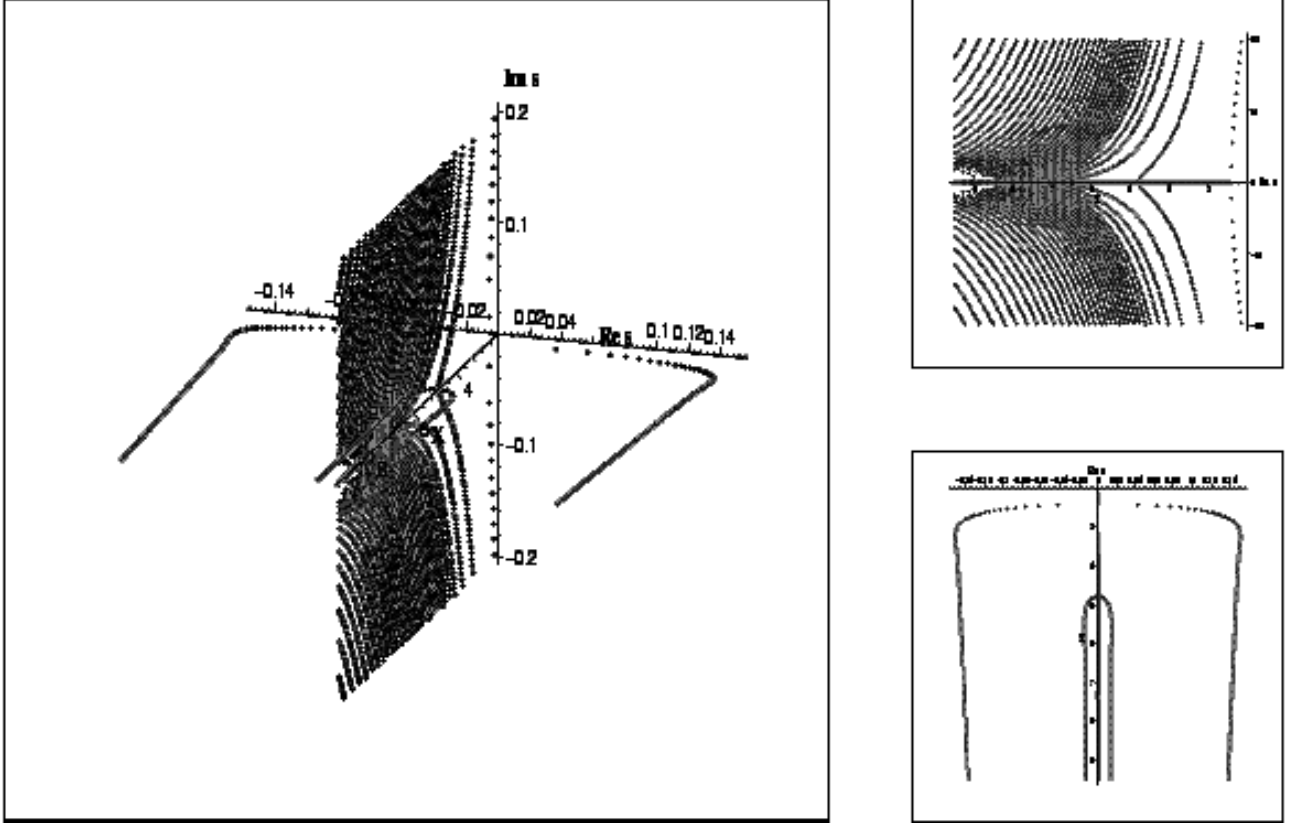


FIG. 1: Spectrum of the modes around the singular isothermal sphere. The real and imaginary parts of the pulsations of the modes are plotted in the 3d-view for a range of values of the size  $X$ . All scales are **logarithmic** ( $\ln(1+x)$  actually). Views from the right and from above are also plotted.

fig.1 since the behaviour of the system is simple there (however  $\ln(X_{c1}/\delta + 1) \sim 2.4$  is visible on the figures). In this regime the modes are oscillating stationary modes and the system is stable. As  $X$  increases above  $X_{c1}$ , the size of the system grows and a first mode encounters a branching point and develops a real positive pulsation. This means that the mode grows exponentially and the system becomes unstable. Then, for successive critical values  $X_{ci}$ ,  $i = 1, 2, \dots$  corresponding to larger and larger sizes of the system, new modes become unstable. It is interesting to mention that the critical values appear when the rate of the larger and lower cutoffs is  $X_{cn}/\delta \sim 10.7^n$ ,  $n = 1, 2, \dots$ . This geometric progression has been found in the thermodynamic study in ref.[11]. When  $X$  goes to infinity, an infinite number of unstable modes appear, which is not surprising since the system then has an infinite mass. Obviously, this limit is unphysical.

Non-radial perturbations have been investigated ( $l \neq 0$ ). These perturbations are always stable and oscillating.

#### D. Stability of the regular isothermal spheres

Regular solutions of eq.(3.1) have been widely studied in spite of the fact that they do not have an analytic expression. In this case it is not necessary to introduce a short distance cutoff in the study of the fluctuations since the background solution is regular at the origin. We keep considering the solution in a large but finite sphere of radius  $X$ . Thus we will use the same boundary conditions as in the singular case, taking  $\delta = 0$ .

We again apply the general numerical method described above. We compute the spectrum of pulsations of the modes for varying values of the size  $X$  of the sphere (see fig.2).

The first point is that the behaviour is very similar to the singular case. The interpretation of fig.2 is the same as that of fig.1. This means that the singular isothermal sphere with short distance cutoff is a good analytic analogue of the regular isothermal sphere. The only difference in the behaviour of the fluctuations is in the specific values of the  $X_{ci}$ . In the regular case, the instability appears at a smaller size ( $X_{c1}/\delta \sim 9.$ ) than in the singular case ( $X_{c1}/\delta \sim 10.7$ ).

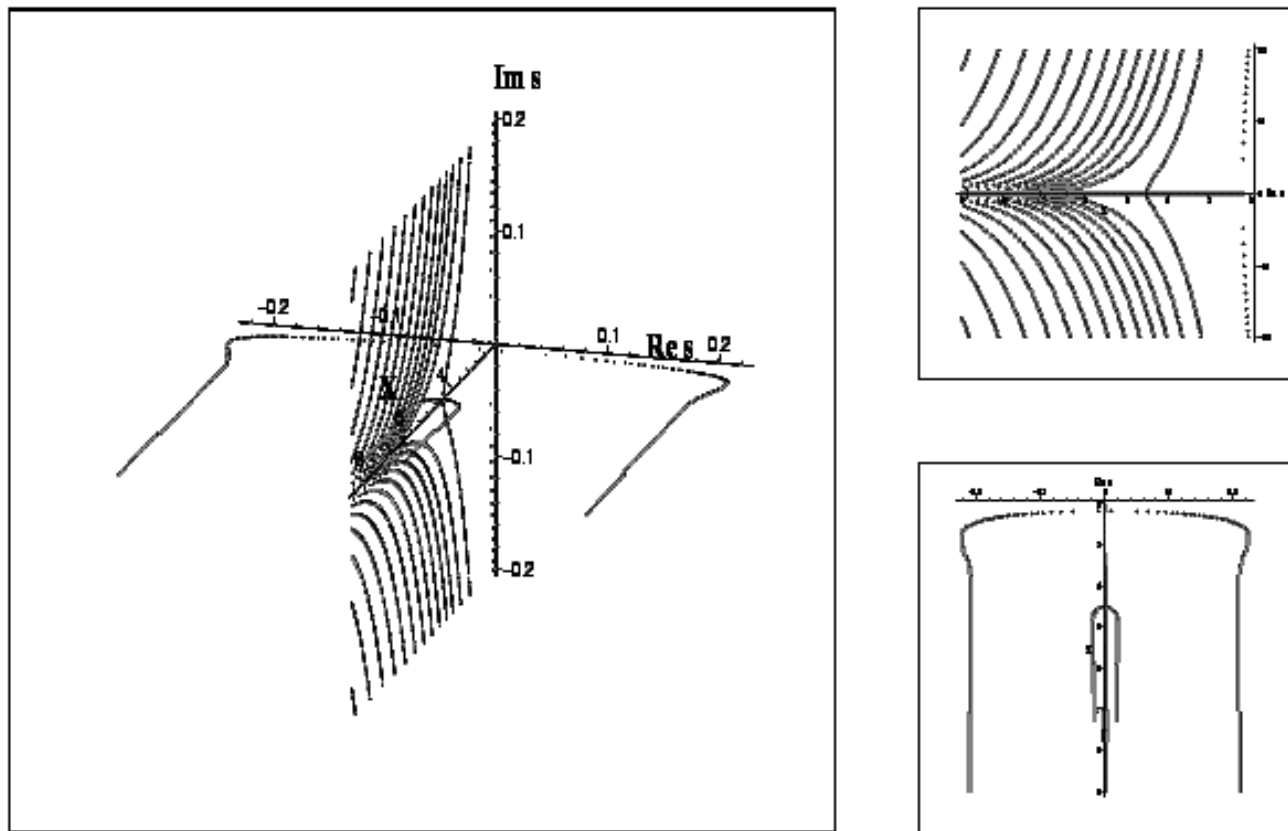


FIG. 2: Spectrum of the modes around the regular isothermal spheres. Explanations are the same as in Fig 1.

As expected, the value  $X_{c1}/\delta \sim 9.0$  corresponds to a ratio of 32.1 between the central and border densities of the background. This critical ratio is the same as in the study of the thermodynamic stability in the canonical ensemble[5]. Finally the numerical study suggests that the ratio 10.7 between two successive  $X_{ci}$  is asymptotically obtained at large  $X$  in the regular case, as it must be.

### E. Profile of the instable modes

Having established that the dynamic instability appears for the same center-to-border density contrast as in the thermodynamic instability, we now check if the profile of the first instable mode matches the profile of the thermodynamic instability, and we investigate the profile of other instable modes.

Those profiles are given, when we use the finite differences method, by the coordinates of the vector of the one-dimensional kernel of our operator (boundary conditions included). For a given size, we are thus able to determine the profile of each mode associated with a zero of the determinant for specific values of  $s$ . On fig. 3 the profiles are given for the first and second instabilities for sizes just above their critical sizes. As can be seen, the first instability is a spherical collapse forming a dense core. Its density profile is similar to the profile of the thermodynamic instability [6]. The second instability combines a core collapse and the ejection of a shell.

## V. EFFECT OF THE VISCOSITY ON THE DYNAMICS AND STABILITY CRITERIA

It is now interesting to establish how viscosity alters the dynamics of the fluctuations. We first proceed to an analytic study of the fluctuations and then perform a thorough numerical analysis.

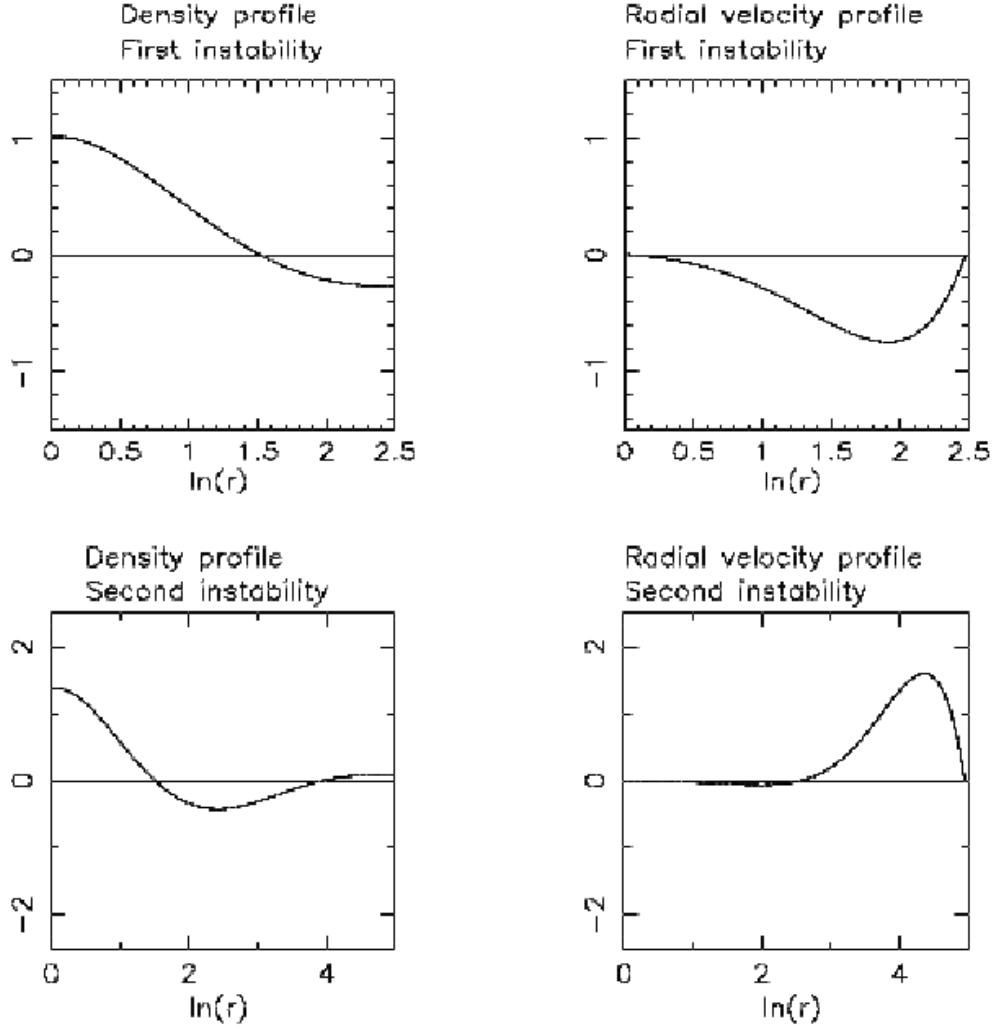


FIG. 3: Radial profiles of the first two instabilities, at sizes just above their emergence, plotted for arbitrary amplitudes.

### A. Analytic study

Here we will study the fluctuations around the singular isothermal sphere with a non-zero viscosity. We consider only radial perturbations since it simplifies the equations and contains the essential information about stability. Using the variables:

$$y = sx, \quad f(y) = \nabla\psi(sx), \quad (5.1)$$

where  $f$  is the (dimensionless) radial velocity, the system (3.14) becomes

$$\left(1 + \frac{1}{s Re} \frac{y^2}{2}\right) \frac{d^2 f}{dy^2} + \frac{y}{s Re} \frac{df}{dy} + \left(\frac{2}{y^2} - 1 - \frac{1}{s Re}\right) f = 0. \quad (5.2)$$

It is interesting to notice that all the dependence on the parameters is through the combination  $s Re$ , which is the turbulent-like Reynolds number associated to a mode of pulsation  $s$ . The asymptotic behaviour of the solutions at large distance is:

$$y \gg 1, y \gg s Re : f(y) = y^{\frac{-1 \pm \sqrt{9 + 8 s Re}}{2}}. \quad (5.3)$$

For  $sRe > -1$ , the component with the upper sign grows at large radius while the other component decays. For negative  $sRe < -1$ , both solutions decay at large radius. The interval  $-1 > sRe > -9/8$  is the only range giving strictly decaying behaviours at large radius. In the other cases ( $sRe < -9/8$  or  $s$  complex) we have spatially oscillating and decaying behaviours. It is easy to check that at small distances one recovers the zero-viscosity solutions. This, of course, does not take the boundary conditions into account. We provide in the next section quantitative results from numerical calculations.

## B. Numerical study

The introduction of the viscosity, although formally cumbersome, fits with no particular difficulty in the finite difference scheme. In particular, it does not change the actual order of the system of differential equations as can be seen from eq.(3.21). The spectrum of modes for a continuous range of the larger cutoff  $X$  can be computed for different values of the Reynolds number. These results are shown on fig.4 and fig.5. We show in fig.6 the evolution of the spectrum at fixed sizes, for a continuous range of values of the Reynolds number.

Obviously, the diagrams are more complex in the viscous case than in the ideal case, especially as we go to Reynolds numbers close to one. Reynolds numbers as small as 0.1 have been investigated but are not plotted since they show no specificity and are unlikely values for a self-gravitating gas. We have three main kind of modes: oscillating-decaying modes, decaying modes, and growing modes. However, all the values of the critical sizes associated with the onset of instabilities are **independent** of the Reynolds number. This can be guessed on fig.5, and checked on fig 6 for  $X_{c1}$ . The stability of the isothermal sphere **does not depend** on the viscosity. Besides, figs.4 and 5 clearly show that the mode associated with the first instability is much less affected by the viscosity than the others.

The real parts of the modes are plotted on fig.6 as functions of the Reynolds number with logarithmic scales, for two different sizes: 10.5 and 11.6 . In the first diagram all modes are stable independently of the Reynolds number and in the second there is exactly one unstable mode for all values of the Reynolds number. This is a confirmation that the dynamic stability criterion depends only on the size of the system and not on the value of the Reynolds number.

## VI. SOLITON-TYPE SOLUTIONS IN THE SELF-GRAVITATING GAS

The appearance of solitons in an isothermal self-gravitating gas has been studied in one spatial dimension in ref.[13]. In this case, the system could be reduced to a sine-Gordon equation. Here we will study the case of axisymmetric soliton-type solutions in  $3 + 1$  dimensions.

### A. Soliton-type equations

We will consider  $z$ -independent solutions of the evolution equations (2.7)-(2.10) without viscosity ( $Re = \infty$ ). It is useful to make the following change of variables,

$$(r, t) \longrightarrow \left( y = \frac{r}{r_0(t)}, t \right), \quad (6.1)$$

where  $r_0(t)$  is a time dependent characteristic length. The simplest non-trivial choice for  $r_0(t)$  is a linear dependence on time. Using the characteristic parameters of the system this leads the soliton variable:

$$y = \frac{\mu r}{1 \pm \mu c_s t} = \frac{x}{1 \pm \tau}. \quad (6.2)$$

We write the potential and radial velocity field as:

$$\Phi = \ln \left[ \frac{f(y)}{(1 \pm \tau)^2} \right], \quad \frac{d\Psi}{dx} = h(y) \pm y. \quad (6.3)$$

Then, the matter conservation equation (2.8) yields

$$\frac{h'(y)}{h(y)} + \frac{1}{y} + \frac{f'(y)}{f(y)} = 0, \quad (6.4)$$

which can be immediately integrated as

$$f(y) h(y) y = \mp C. \quad (6.4)$$

The symbol  $\mp$  in front of  $C$  is introduced for later convenience. Each possibility is associated with one of the choices for the soliton variable.  $C$  going to zero means that the density goes to zero. Inserting eqs.(6.3) and (6.4) in the Euler equation of motion (2.7) gives the non linear equation:

$$h \left( y \left( h h' \pm h - \frac{h'}{h} \right) \right)' = \pm C. \quad (6.5)$$

It is possible to derive some analytic solutions of this equation.

### B. Analytic solutions

The simplest solution to eq.(6.5) is  $h(y) = \mp \sqrt{C}$ . In terms of physical fields this produces non-trivial solutions:

$$\Psi'_0(r, t) = \pm c_s \left( -\sqrt{C} + \frac{r}{\mu^{-1} \pm c_s t} \right), \quad \Phi_0(r, t) = \ln \left[ \frac{-\sqrt{C}}{\mu^2 r^2 (1 \pm \mu c_s t)} \right] = \ln \frac{2}{x^2} + \ln(\sqrt{C} y). \quad (6.6)$$

These two solutions are filaments, one expanding and the other collapsing in a finite time. This solution is invariant under the following scale transformations

$$C \longrightarrow \lambda C, \quad c_s \longrightarrow \frac{c_s}{\lambda}, \quad \mu \longrightarrow \lambda \mu. \quad (6.7)$$

Hence, in the calculation of the fluctuations [sec. VI C], we can set for example  $\sqrt{C} = 1$ .

Guided by numerical integration (see fig. 7), another type of solution can be found for low densities. It is possible to build a perturbative solution of eq.(6.5) around the exact solution  $C = 0$ ,  $h(y) = \mp y$ . Since the system is ill-defined at  $C = 0$ , we will consider  $C \ll 1$  and we will develop  $h(y)$  perturbatively in  $C$ .

$$h(y) = \mp y [1 + C h_1(y) + \mathcal{O}(C^2)] . \quad (6.8)$$

Then  $h_1(y)$  obeys the simple equation:

$$y^2 h_1 + y(y^2 - 1) h_1' = \pm \ln \frac{B}{y}, \quad (6.9)$$

which has the general solution,

$$h_1(y) = \frac{1}{\sqrt{|y^2 - 1|}} \left( A \pm \int \frac{dy \ln \left( \frac{B}{y} \right)}{y \sqrt{|y^2 - 1|}} \right). \quad (6.10)$$

We see that in general  $h_1(y)$  is singular at  $y = \pm 1$ , that is, on the wavefront  $x = |1 \pm \tau|$ . Regular solutions can be obtained by appropriate choices of  $A$  and  $B$ . We plot in fig.(7) a regular solution  $h_1(y)$  for  $B = 1$ .

We obtain from eqs.(6.8) and (6.10) the physical fields:

$$\Psi = \pm c_s C y h_1(y) \quad , \quad \Phi = \ln \left\{ \frac{C}{x^2} [1 - C h_1(y)] \right\} . \quad (6.11)$$

It is important to notice that this perturbative development fails at short distances ( $y \rightarrow 0$ ) where the density is not small anymore.

### C. Fluctuations around a soliton-like solution

We intend to assess the stability of the solution (6.6). By stability we mean that the growth of the fluctuations should be slower than the growth of the background.

We compute here the explicit form of the radial fluctuations around the soliton-like solution described by eq.(6.6). The collapsing filament case is studied. We define the two independent variables:

$$y = \frac{x}{1 - \tau}, \quad z = 1 - \tau. \quad (6.12)$$

We consider the perturbative expansion

$$\Phi(x, \tau) = \Phi_0 + \epsilon f(y, z), \quad \frac{d\Psi}{dx}(x, \tau) = \frac{d\Psi_0}{dx} - c_s \epsilon g(y, z). \quad (6.13)$$

We can then linearize the evolution equations and we find

$$\sqrt{C} y \frac{\partial^2 g}{\partial y^2} - y z \frac{\partial^2 g}{\partial y \partial z} - (-\sqrt{C} + y) \frac{\partial g}{\partial y} - z \frac{\partial g}{\partial z} - g = y \frac{\partial^2 f}{\partial y^2} + \frac{\partial f}{\partial y} + \sqrt{C} f, \quad (6.14)$$

$$-\sqrt{C} \frac{\partial f}{\partial y} + z \frac{\partial f}{\partial z} + \frac{\partial g}{\partial y} = 0. \quad (6.15)$$

These equations are homogeneous in  $z$  so their solutions can be written as a sum of solutions of the type:

$$f(y, z) = f(y) z^\alpha, \quad g(y, z) = g(y) z^\alpha, \quad \alpha \in \mathbb{C}. \quad (6.16)$$

Inserting these expressions in eqs.(6.14) and (6.15) and eliminating  $g$ , gives an equation for  $f$ :

$$x(C-1)f''' + [2(C-1) - (2\alpha+1)\sqrt{C}x]f'' + [-(4\alpha+3)\sqrt{C} + \alpha(\alpha+1)x]f' + 2(\alpha+1)\alpha f = 0. \quad (6.17)$$

This equation can be integrated in the general case. However, according to the transformation (6.7) we can choose the case  $\sqrt{C} = 1$ . In this case the solutions take the following form:

$$f(y) = B_1 \Phi(\lambda_1, \nu_1, \beta y) + B_2 y^\gamma \Phi(\lambda_2, \nu_2, \beta y). \quad (6.18)$$

where,

$$\lambda_1 = 2, \quad \nu_1 = 2 + \frac{1}{1+2\alpha}, \quad \lambda_2 = \frac{2\alpha}{2\alpha+1}, \quad \nu_2 = \frac{-1}{2\alpha+1}, \quad (6.19)$$

$$\beta = \frac{\alpha(\alpha+1)}{2\alpha+1}, \quad \gamma = -1 - \frac{1}{2\alpha+1}. \quad (6.20)$$

Here  $\Phi(\lambda, \nu, y)$  stands for the confluent hypergeometric function. It is regular at  $y = 0$  and grows exponentially for  $y \rightarrow \infty$ . Expression (6.18) is degenerate for  $\alpha = -\frac{1}{2}$ :

$$\alpha = -\frac{1}{2}, \quad f(y) = \frac{B}{1 + \frac{y}{4}}. \quad (6.21)$$

According to (6.16), it diverges when the time  $\tau$  reaches 1.

Another degenerate case is  $\alpha = -1$ ,

$$\alpha = -1, \quad f(y) = y \left[ \ln\left(\frac{B_1}{y}\right) + 1 \right] + B_2. \quad (6.22)$$

Interestingly,  $Re(\alpha) \in [-1, -\frac{1}{2}]$  are the only values of  $\alpha$  where the fluctuations are regular at  $y = 0$ . But again the fluctuations diverge for  $\tau \rightarrow 1$ .

Since the fluctuations are ill-behaved for  $y \rightarrow \infty$  and often at  $y = 0$ , we resort to the same method as in the singular isothermal sphere. We define a large distance cutoff  $X$  and a small distance cutoff  $\delta$  for  $y$  and we set the fluctuation to zero on these walls. It should be noted that these walls move with the soliton, and that they cannot be considered as physical since the constant component of the background velocity field flows through the walls. However, those cutoffs allow us to search for fluctuations as eigenmodes in the same way we did for isothermal spheres. These modes appear for special values of  $\alpha$  defined here again by the cancellation of a determinant:

$$\Phi(\lambda_1, \mu_1, \beta\delta)X^\gamma\Phi(\lambda_2, \mu_2, \beta X) - \Phi(\lambda_1, \mu_1, \beta X)\delta^\gamma\Phi(\lambda_2, \mu_2, \beta\delta) = 0 \quad (6.23)$$

These cancellations must be investigated in the complex plane for  $\alpha$  and for various values of  $\frac{X}{\delta}$ . The results appear on fig. 8. The main result is that modes with  $Re(\alpha) < 0$  exist for all values of  $\frac{X}{\delta}$  investigated. These modes have a faster growth than the background. Besides,  $\frac{X}{\delta} \sim 4.5$  is a special value for the radial size of the system. Below this value all the unstable modes have the following time behaviour

$$(1 - \tau)^{\alpha_1} \cos[\alpha_2 \ln(1 - \tau) + \phi]$$

that is, growing oscillations. Above this value  $\frac{X}{\delta} \sim 4.5$  two modes appear that have a pure power law behaviour in time. These modes have larger exponents than the others, that is to say they grow faster. Moreover, just above this critical value, the exponent in the power law seems to go to  $-\infty$ , which indicates a strong instability.

We must keep in mind the fact that this is a partial analysis. Indeed our fluctuations are invariant along the  $z$  symmetry axis. This means that they have an infinite mass. If the size of the system along the  $z$  symmetry axis was bounded and fluctuations with  $r$  and  $z$  dependence computed, a stable region would certainly appear for small enough sizes. We believe that the value  $\frac{X}{\delta} \sim 4.5$  is actually connected to the onset of a *radial* instability, while below this value the growth of the modes is due to the axial infinite size of the fluctuations.



## VII. CONCLUSIONS

In the first part of this work we have described a general method to study the dynamic stability of stationary configurations of self-gravitating fluids and applied it to the isothermal spheres. The interest of this method is that it can be applied to any stationary field. Moreover, we have shown that it is perfectly able to handle viscosity. We have applied this dynamical stability analysis to a stationary solution, the isothermal sphere. In this case we have found a series of sizes ( $X_{c_n} \sim 10.7^n$ ,  $n = 1, 2, \dots$ ) associated with the appearance of instable modes. The size associated to the first instable mode matches the critical size found in the thermodynamic theory. Moreover, we have shown that the values of these sizes are independent of the Reynolds number.

In the second part of this paper we studied exact dynamical solutions. We have presented elements of a soliton theory for a self-gravitating perfect isothermal fluid with axial symmetry. This method provides new dynamic exact solutions. We have analyzed the stability of one of these solutions, a collapsing filament, with a method similar to the method used for the isothermal sphere. Here again we have found that a critical radial size appears to define two regimes. Above this size the system is unstable. Below, it is weakly unstable and may in fact be stable if the axial size of the system was bounded.

These two studies are complementary descriptions of the dynamics of the self-gravitating fluid. One description deals with a stationary background and the other with a dynamical one. Although the first description obeys spherical symmetry and the second obeys axial symmetry, they are closely connected by their structure. Indeed, the density field of eq.(6.6) is the sum of two terms:  $\ln(2/\mu^2 r^2)$  (identical to the stationary spherical solution) and a second term,  $\ln \left[ \frac{\sqrt{C}}{1 \pm \mu c_s t} \right]$ , function of the soliton-time variable alone. In the stationary case, the instability appears when a mode is growing; in the dynamical case, it appears when a mode is growing faster (or decaying slower) than the evolving background solution. In this respect, the stability of the solution in both cases is governed by Jeans-like instabilities whose emergence depends only on the size of the system. We showed that the existence of a critical size does not only apply to stationary solutions but to dynamic solutions as well.

Finally, we would like to add that it is probably possible to give a more general formulation of the soliton-type equations of the system, following on the results in ref.[13] in the one dimensional-case. For example, the choice of the soliton variable in our work, eq.(6.2), is probably a particular case of a more general change in the variables. In any case, the soliton methods provide a powerful approach to self-gravitating fluid dynamics which certainly deserves more investigation.

- 
- [1] Ya. B. Zeldovich and I. D. Novikov, ‘Relativistic Astrophysics’, Univ. of Chicago Press, 1983.
  - W. C. Saslaw, ‘Gravitational Physics of Stellar and Galactic Systems’, Cambridge U. Press, 1987.
  - [2] S. Chandrasekhar, *An introduction to the study of stellar structure*, New York, Dover, (1939).
  - [3] V. A. Antonov, Vest Lenin Univ, **7**, 135 (1962)
  - [4] D. Lynden-Bell and R. Wood, MNRAS, **138**, 495-525 (1968)
  - [5] G. Horwitz and J. Katz, **211**, 226 (1977) and ApJ, **222**, 941-958 (1978)
  - [6] T. Padmanabhan, Phys Rep, **188**,5, 285-362 (1990)
  - [7] L. Landau and E. Lifchitz, Mécanique des Fluides, Eds. MIR, Moscou 1971.
  - [8] L. Hernquist and N. Katz, ApJ Sup, **70**, 419 (1989)
  - [9] H. J. de Vega, N. Sánchez and F. Combes, Nature, **383**, 56 (1996), Ap. J. **500**, 8 (1998).
  - [10] H. J. de Vega, N. Sánchez and F. Combes, Phys. Rev. **D54**, 6008 (1996).
  - [11] B. Semelin, H. J. de Vega, N. Sánchez and F. Combes, Phys. Rev. **D59**, 125021, (1999)
  - [12] H. J. de Vega and N. Sánchez, hep-th/9903236, Phys. Lett. **B490**, 180 (2000).
  - [13] G. Götz, Class Quantum Grav, **5**, 743-765 (1988)
  - [14] S. Inutsuka and S. M. Miyama, Ap J, **388**, 392-399 (1992)
  - [15] G. Petiau, ‘La théorie des Fonctions de Bessel’, CNRS, Paris, 1955. See page 181.
  - [16] H. R. Beyer and B. G. Schmidt, A & A, 296, 722 (1995).
  - H. R. Beyer and K. D. Kokkotas, Mon. Not. R. Astron. Soc. 308, 745 (1999).
  - [17] R. Courant and D. Hilbert, Method of Mathematical Physics, vol. 1, J. Wiley, New York, 1965.

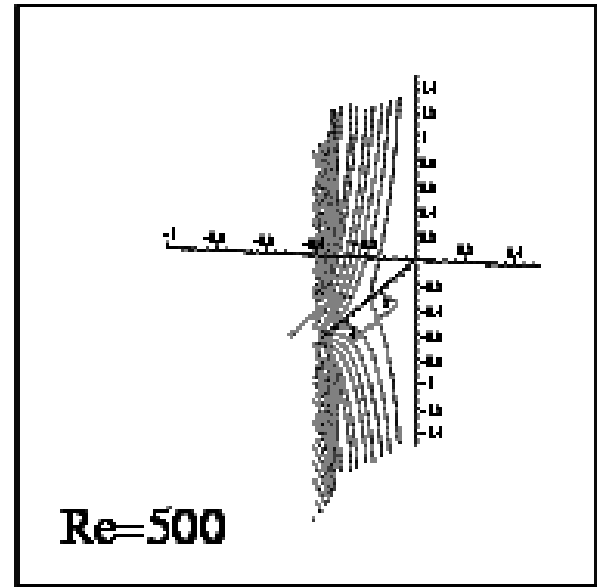
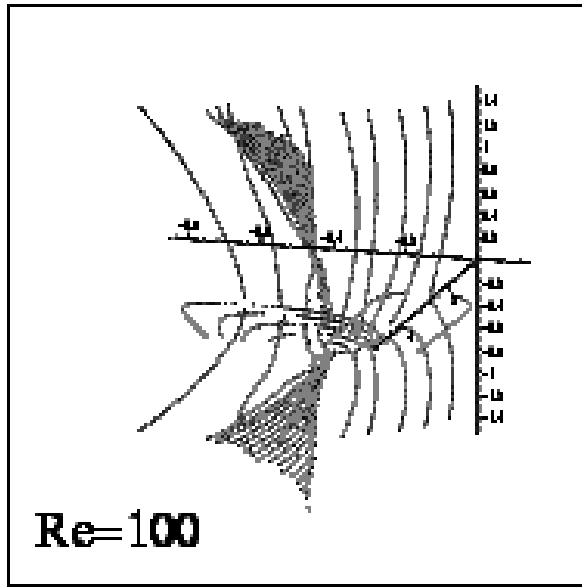
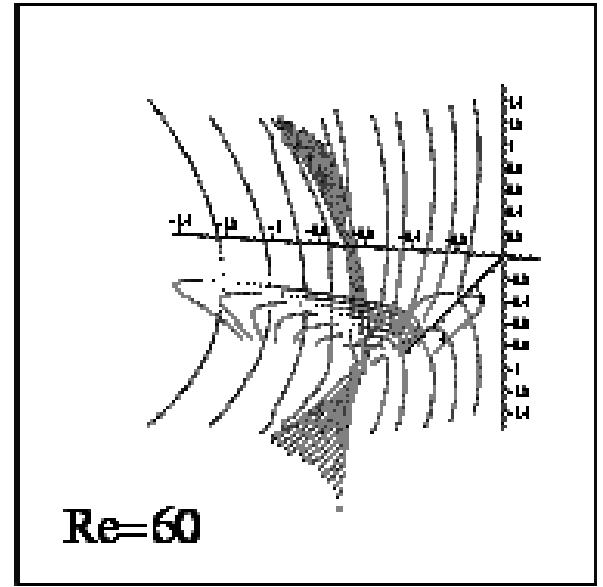
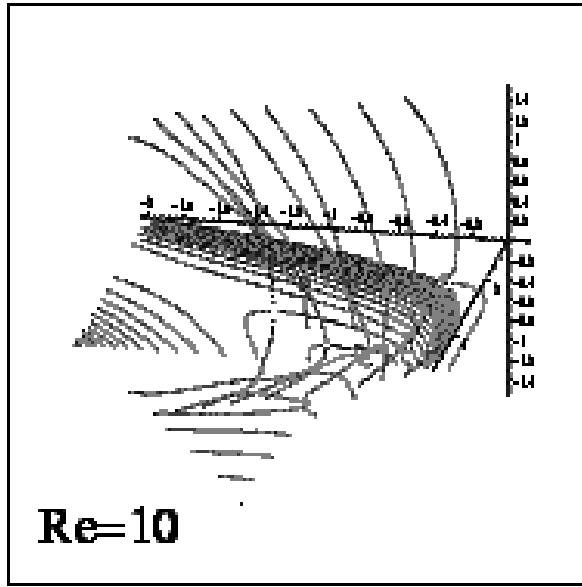


FIG. 4: Spectrum of viscous modes around the singular isothermal sphere. The real and imaginary parts of the pulsations of the modes are plotted in 3d-views for a range of values of the size  $X/\delta$ , and four values of the Reynolds number. All scales are logarithmic.

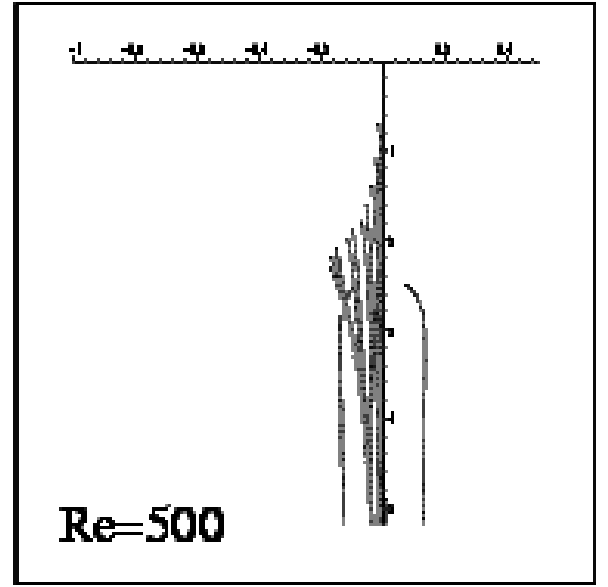
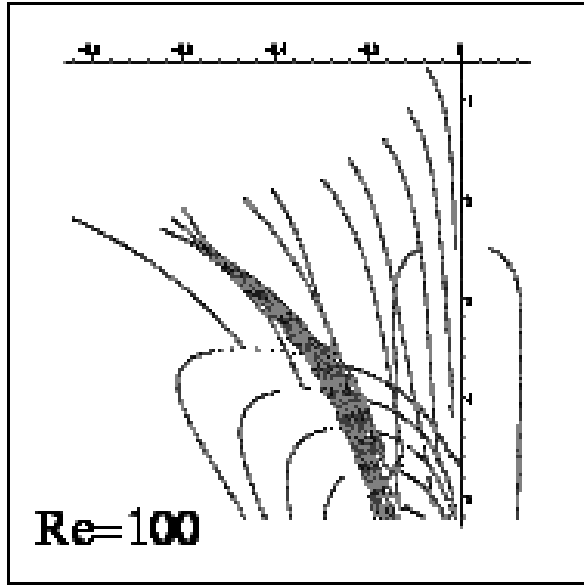
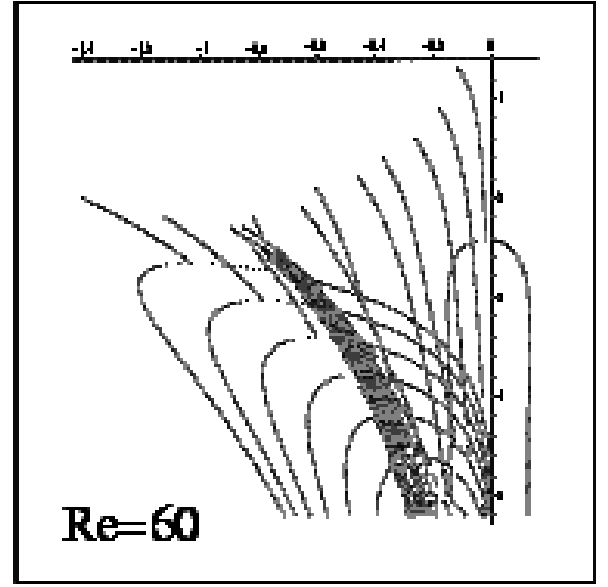
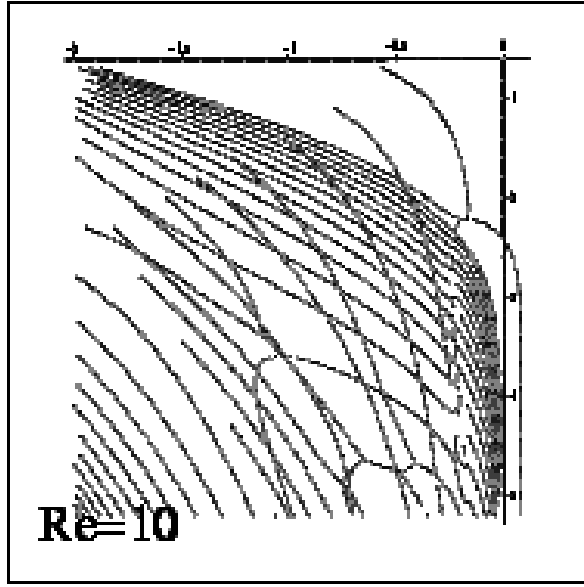


FIG. 5: Upper views of fig. 4. The real parts of the pulsations of the modes appear as functions of the ratio  $X/\delta$ . Positive real parts appear for the same values of  $X/\delta$  ( $\ln(1 + X/\delta) \sim 2.4$ ), independently of the Reynolds number.

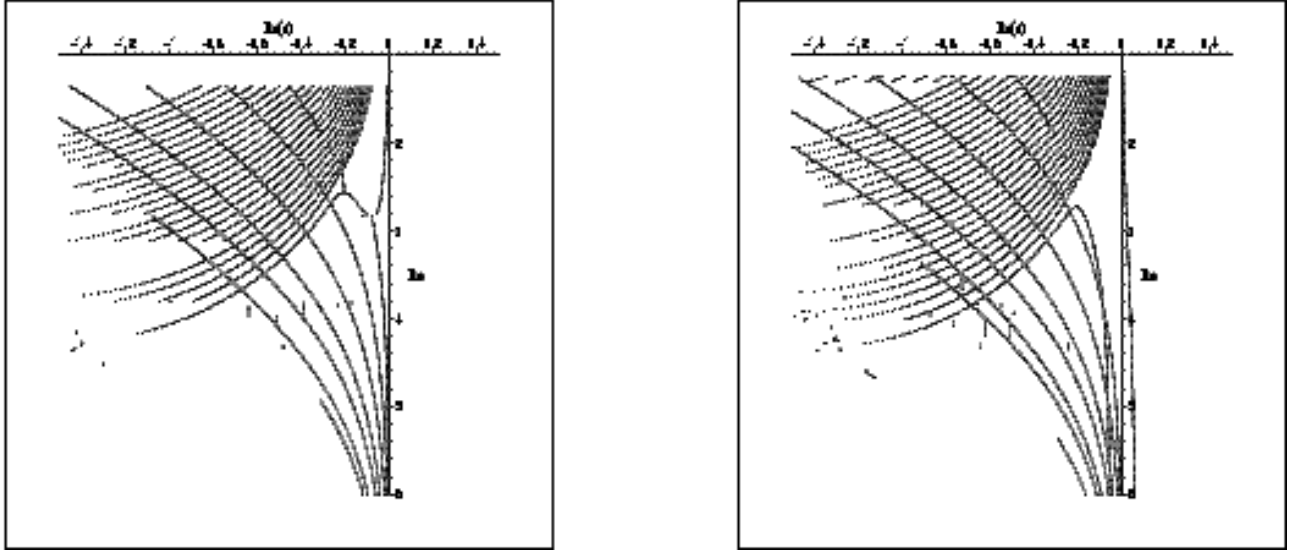


FIG. 6: The real parts of the pulsations of the modes are plotted as functions of the logarithm of the Reynolds numbers for fixed sizes: 10.5 on the left and 11.6 on the right.

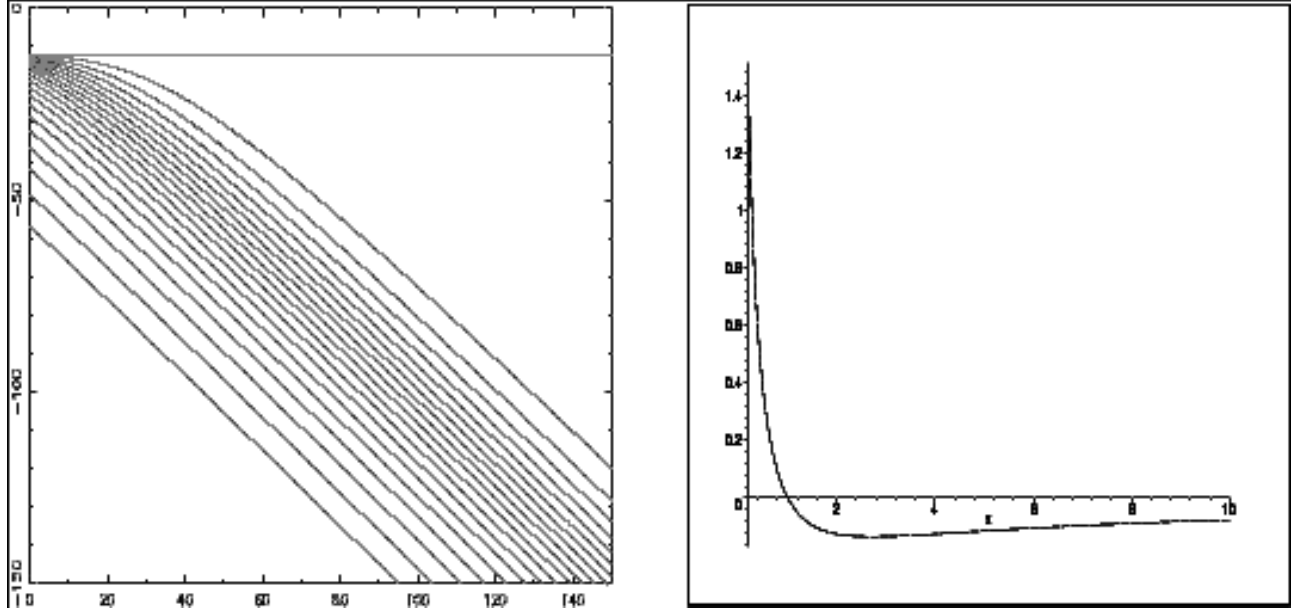


FIG. 7: On the left solutions of eq.(6.5) are plotted for various initial conditions. On the right the function  $h_1$  is plotted for  $B = 1$ .

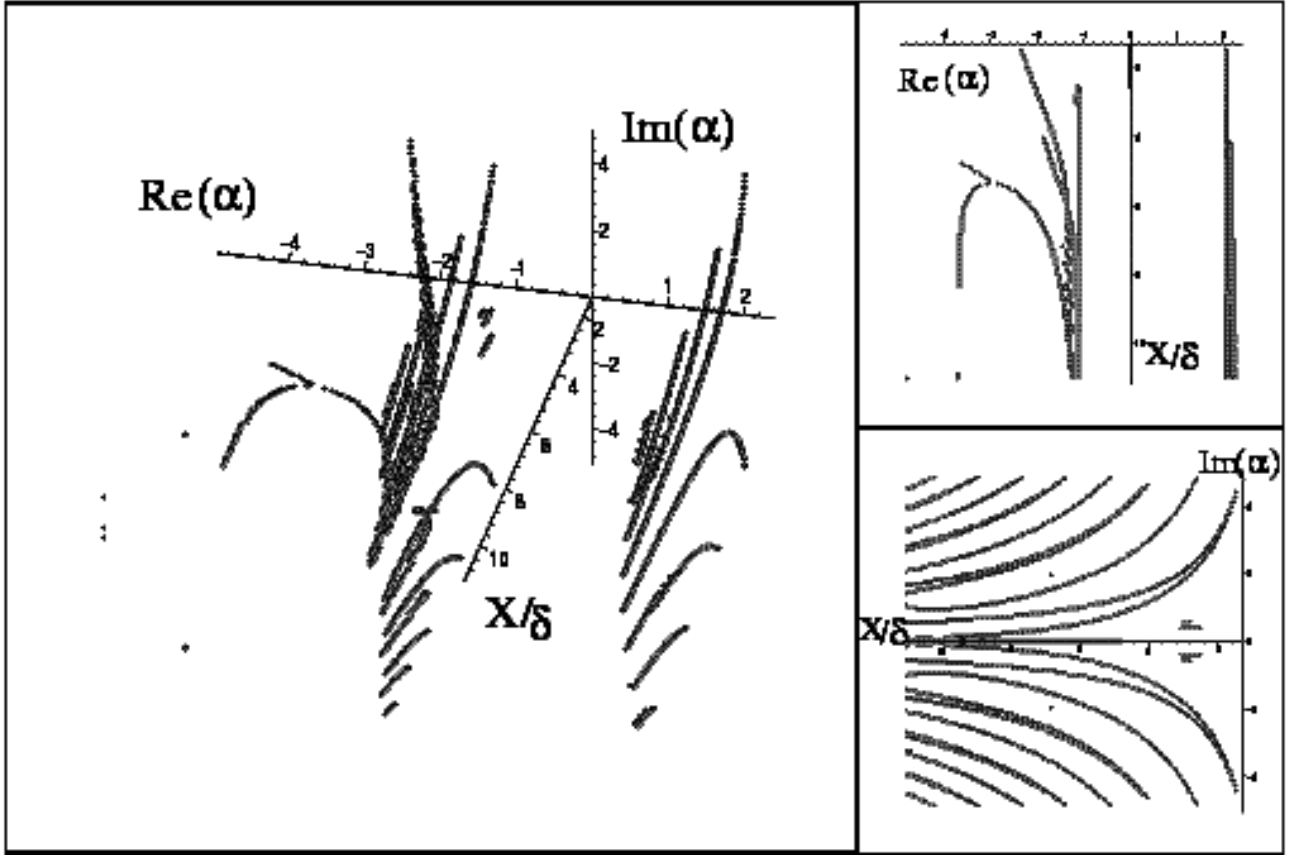


FIG. 8: Spectrum of modes around solution (6.6) for a continuous range of values of  $\frac{R}{\delta}$ . The real and imaginary parts of  $\alpha$  are plotted against  $\frac{R}{\delta}$ .